DOI: 10.1016/S1872-5813(22)60063-X

Effects of metal doping on the catalytic performance of LaFe-based perovskites for CO_2 hydrogenation to light olefins

MA Li-hai , GAO Xin-hua , ZHANG Jian-li* , MA Jing-jing , HU Xiu-de , GUO Qing-jie*
(*State Key Laboratory of High-effciency Utilization of Coal and Green Chemical Engineering, College of Chemistry & Chemical Engineering, Ningxia University, Yinchuan* 750021, *China*)

Abstract: The catalytic behavior of K/$LaFeBO_3$ (B =Cu, Zr, Al, Mn, Ni, and Zn) perovskite catalysts prepared by sol-gel and impregnation methods was investigated for CO_2 hydrogenation to light olefins. The structure of various catalysts was characterized in detail by SEM, XRD, N_2 adsorption-desorption, H_2-TPR, CO_2-TPD, TG, and XPS analysis. With the addition of Cu and Zn, the particles size decreased with high dispersion of Fe, while the exposed basic sites increased with lower hydrogen desorption temperature. The oxygen mobility in perovskites exhibited a considerable impact on catalytic activity and olefins selectivity, which considerably increased when Fe was substituted by Cu and Zn at the B site. Olefins were formed preferentially from oxygen species of the surface lattice with low binding energies (BEs). In addition, a faster diffusion rate of oxygen would lead to an enrichment of lattice oxygen species on the surface and increase the production of olefins.

Key words: CO_2 hydrogenation; perovskite; $LaFeBO_3$ catalyst; oxygen mobility
CLC number: TQ546 **Document code:** A

Carbon dioxide (CO_2) capture and usage has received a lot of interest with the concerns of global warming and climate change. By integrating CO_2 capture and conversion, chemical looping combustion (CLC) presents a revolutionary strategy for reducing CO_2 emission and increasing its utilization. Chemical conversion of CO_2 by hydrogenation to methanol, light olefins ($C_2^= - C_4^=$) and other chemicals has attracted great attention. Especially, many progresses have been achieved for CO_2 selective hydrogenation to light olefins[1−4].

Two independent reactors make up the CLC system[5]. During the CLC process, fuel reduces metal oxide to a reduced state in a combustion reactor, whereas oxygen oxidizes the reduced state to an oxidized state in an air reactor. Fe-based perovskite composites can be used as oxygen carrier with promising CLC performance[4]. In addition, the reduced Fe-based composite in the outlet of combustion reactor can be applied for CO_2 hydrogenation via reverse water gas shift reaction (RWGS) and Fischer-Tropsch synthesis (FTS) to light olefins in a hydrogenation reactor. The hydrogenation-induced phase shift of iron oxides occurs between different reactors (Figure 1). The construction of oxygen carrying carrier and CO_2 activation bifunctional active centers of Fe-based oxygen carriers is the key to the coupling technology of chemical looping CO_2 capture and its utilization.

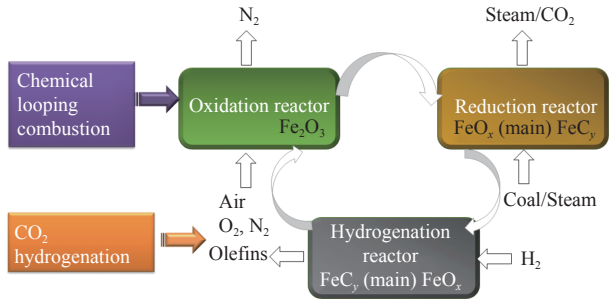

Figure 1 Schematics of chemical looping coupled hydrogenation process

The deactivation of metal oxide during numerous redox cycles is the key problem to be solved in CLC process[5,6]. A crucial point in developing chemical looping coupled with CO_2 hydrogenation systems is the selection of a high-performance oxygen carrier that can be reduced and oxidized repeatedly without deactivation. Fe-based catalysts have already been employed for the CO_2 hydrogenation reaction. CO_2 hydrogenation over Fe-based catalysts is generally based on a RWGS-FT process, during which CO is firstly generated by reverse water-gas shift (RWGS),

Received: 2022-05-30; Revised: 2022-07-28

* Corresponding author. E-mail: zhangjl@nxu.edu.cn, qingjie_guo@163.com.

The project was supported by the Key Project of Natural Science Foundation of Ningxia (2022AAC02002) and the National Natural Science Foundation of China (U20A20124).

followed by CO hydrogenation to various hydrocarbons via FT reaction[3]. However, the sole Fe-based catalysts always possess poor selectivity to light olefins and are prone to deactivate due to carbon deposition and sintering. Many metal promoters have been introduced for CO_2 conversion to increase the selectivity to light olefins[7]. For example, with the addition of copper, less methane was formed with higher activity[8]. Mn promoter, on the other hand, can considerably reduce the production of carbon deposition and improve catalyst stability[9]. By encouraging additional lattice oxygen vacancies and electron pairs for the catalyst, Zn can improve the activity of Fe catalysts[10]. The basicity of the catalyst surface can be adjusted by Al and Zr to ensure adequate CO_2 adsorption. The addition of Ni with a high hydrogenation capability also enhanced CO_2 conversion and the production of more active metals[7,11−13]. Additionally, alkali metals including sodium and potassium can be used as electron promoters to provide electrons to the *d* empty orbitals of iron or other metals, effectively promoting CO_2 adsorption while suppressing hydrogen adsorption. As a result, methane formation was suppressed to benefit light olefin production[14].

Perovskite oxides with ABO_3 structure can be considered as an acid-base catalyst with the presence of both metal (cationic) and oxygen (anionic) vacancies, which can tackle the problem of rapid deactivation caused by metal particle aggregation at high temperatures. Some perovskite oxides have been successfully applied for chemical looping coupling RWGS process[15,16]. It was suggested that the oxidation state mismatch in the ABO_3 structure causes charge imbalance and increases oxygen vacancy. The modification of transition metal on iron-based perovskite oxides enhanced the stabilization of the anomalous cationic oxidation state in the RWGS process by increasing the contact strength between active species and carriers. However, the specific surface area of perovskite oxides is always rather low with few active sites, which limits reactant absorbtion and thus decreased the activity. After reduction treatment and under reaction procedures, the perovskite is partially reduced. Reduced lattice cations move to the surface, where they exsolve and form metallic nanoparticles[17]. During CO_2 activation, C−O bond breaks on the catalyst surface, and the resulting oxygen atom diffuses into the bulk. Some studies have indicated that the nanoparticles formation by exsolution improved sintering stability due to “anchoring”, even at high reaction temperature.

Due to the complexity of the chemical compositions, topologies, and phases, the reduction and activation ability of perovskites with ABO_3 structure in CO_2 hydrogenation need to be further investigated. In this study, the catalytic behavior of $LaFeBO_3$ perovskite catalysts (B= Cu, Zr, Al, Mn, Ni, and Zn) in CO_2 hydrogenation was investigated. Detailed characterizations were used to establish the correlation between the catalytic performance and structure. The anchoring effect of reduced metal nanoparticles on oxygen mobility and olefin selectivity was also discussed.

1 Experimental

1.1 Catalysts preparation

Sol-gel and impregnation methods were used to prepare K/$LaFeBO_3$ (B =Cu, Zr, Al, Mn, Ni, Zn) catalysts. Typically, an adequate amount of various metal nitrates and citrate acid were dissolved in deionized water to form a mixed salt solution with molar ratios of La∶Fe=2 and Fe∶B=1. The prepared solution was then heated and stirred in 80 °C water bath for gel formation, which was then dried in an oven at 105 °C for 12 h. The dried samples were calcined at 400 °C for 1 h and 750 °C for 5 h, under static air with a ramp of 5 °C/min. The obtained perovskites were denoted as $LaFeBO_3$ (B=Cu, Zr, Al, Mn, Ni, and Zn). Finally, the samples were impregnated with potassium carbonate (2%).

1.2 Structure characterizations

Scanning electron microscopy (SEM, KYKY-2008B) was used to examine the morphology of all fresh and used catalysts at a voltage of 25 kV.

X-ray diffraction (XRD) patterns were conducted using monochromatic Cu *Kα* radiation and a Rigaku D/MAX2200PC spectrometer at 40 kV and 30 mA. The samples were scanned from 5° to 80° with scanning rate of 8(°)/min.

N_2-physisorption measurement was carried out on a Micrometrics ASAP2460 instrument after all catalysts were vacuum purged at 300 °C for 3 h. The specific surface areas, average pore diameters, and pore volumes of the catalyst samples were obtained by Brunauer-Emmet-Teller and Barrett-Joyner-Halenda methods.

H_2 temperature-programmed reduction (H_2-TPR) was tested using a Micromeritics AutoChem II 2920 chemisorption analyzer with a thermal conductivity

detector (TCD). 50 mg of sample in a quartz tube was first flushed with He (30 mL/min) at 350 °C for 1 h to remove moisture before cooling to 50 °C. After that, the temperature was raised to 800 °C at a rate of 10 °C/min with a flow of 10% H_2/Ar. The H_2 consumption was recorded simultaneously.

Temperature-programmed CO_2 desorption (CO_2-TPD) was performed in-situ on a Micromeritics AutoChem II Chemisorption Analyzer. A 50 mg sample was reduced by 10% H_2/Ar for 800 °C before being purged for 1 h with He (30 mL/min). After cooling in a He flow, the sample was pulse-adsorbed by CO_2 at 50 °C until saturation was obtained, followed by being purged with He for 1 h. The desorption signal was captured while the temperature was raised from 50 to 800 °C at a rate of 10 °C/min.

Thermogravimetric analysis was carried out using an SDT Q600 simultaneous thermal analyzer (TA instruments). Under CO atmosphere, the weight loss of the catalysts was measured from room temperature to 800 °C at a heating rate of 10 °C/min.

The elemental composition of the sample was analyzed by Agilent-5110 measurement as an energy dispersive X-ray spectrometer.

X-ray photoelectron spectroscopy (XPS) for all catalyst samples was performed with an Al *K*α X-ray source using a Thermo Scientific ESCALAB 250 spectrometer. The base pressure in the chamber was less than 2×10^{-8} Pa. The C 1*s* peak at 284.8 eV was used to calibrate binding energies (BEs) in relation to adventitious carbon.

1.3 Catalytic performance evaluation

The catalytic performance for CO_2 hydrogenation over various samples was tested in a stainless steel fixed-bed reactor (i.d.=8 mm; length=400 mm). 1 mL of catalyst and 2 mL of quartz sand were packed in the centre of the tube with a thermocouple in contact with the catalyst to measure the temperature of the catalyst bed. The perovskite was reduced for 4 h at 800 °C in H_2 flow prior to the catalytic test. CO_2 hydrogenation was carried out at t=320 °C, p=2.0 MPa, GHSV=1000 h^{-1}, and H_2/CO_2=3 (molar ratio). The gaseous products and reactants were detected using an online gas chromatograph (GC-9560) with a TCD and a flame ionization detector. The product selectivity was calculated on a carbon basis. CO_2 conversion (x_{CO_2}) and product selectivity (s_i) were calculated by Eqs. (1) and (2):

$$x_{CO_2} = (F_{in} \cdot Y_{CO_2,in} - F_{out} \cdot Y_{CO_2,out})/(F_{in} \cdot Y_{CO_2,in}) \times 100\% \quad (1)$$

$$S_i = (F_{out} \cdot Y_{i,out} - F_{in} \cdot Y_{i,in})/(F_{in} \cdot Y_{CO_2,in}) \times 100\% \quad (2)$$

where F_{in} and F_{out} are the molar flows of the feed gas and effluent (mol/h), respectively; $Y_{CO_2,in}$ and $Y_{CO_2,out}$ are the volume fractions of CO_2 in the feed gas and effluent, respectively; and $Y_{i,in}$ and $Y_{i,out}$ are the volume fractions of hydrocarbons in the feed gas and effluent, respectively.

2 Results and discussion

2.1 XRD measurement

The typical formula for perovskite oxides is ABO_3, with large ions occupying the 12-coordinated A sites (r_A>0.90 Å) and transition-metal cations occupying the 6-coordinated B sites (r_B>0.51 Å). Because of the extraordinary stability of the perovskite structure, many metals with differing oxidation states can be partially substituted for the cations in the A or B sites, resulting in structural defects such as cationic or anionic vacancies[18]. Figure 2 shows the diffraction peaks of $LaFeO_3$ perovskite structure (JCPDS 37-1493). When Cu, Mn, Zn, Al, and Zr are doped, the $LaFeO_3$ structure can be well preserved. However, the intensity of diffraction peaks is weakened and new phases including $ZnFe_2O_4$, $FeAlO_3$, and $La_2Zr_2O_7$ are formed. In addition, doping Ni in $LaFeO_3$ caused the formation of NiFe alloy. The orthorhombic perovskite structures with the (121) characteristic reflection peak can be observed. Partial substitution of the B site results in a smaller pseudo cubic unit cell for perovskite structure with a slight shift to higher 2θ degree. As shown in Table 1, compared with $LaFeO_3$, the crystalline size calculated by Scherrer equation decreased when different metals were doped. The grain size was found to be 14.8 nm when Mn was doped, while a higher grain size of 30.8 nm was obtained by Cu doping.

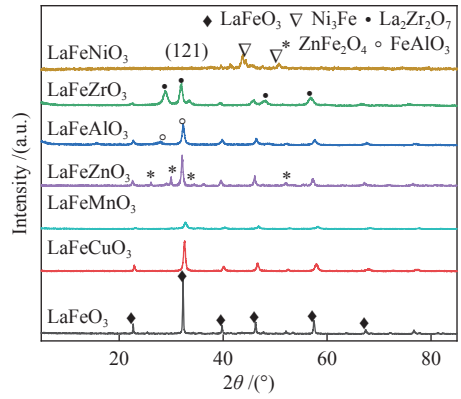

Figure 2　XRD patterns of the calcined catalyst samples

Table 1 Crystalline size of various catalyst samples

Catalyst	Crystalline size/nm[a]	Lattice parameter/ Å
$LaFeO_3$	96	3.5628
$LaFeMnO_3$	14.8	3.8754
$LaFeCuO_3$	30.8	3.8903
$LaFeAlO_3$	16.7	4.4676
$LaFeZrO_3$	22.8	3.6622
$LaFeZnO_3$	28.9	4.6819
$LaFeNiO_3$	29.8	6.4846

[a]: Caculated by Scherrer equation

2.2 Textural properties

SEM images of the $LaFeBO_3$ catalysts revealed the existence of mesoporous structure (Figure 3), which was further evidenced by N_2 physisorption data (Figure 4). It can be seen that $LaFeO_3$ is made up of closely packed sphere-like nanoparticles with an average particle size of 80–100 nm (Figure 3(a), (b)). Small pores on the particle surface following Zr doping, as shown in Figure 3(f), may be caused by nitrate thermal decomposition. It produces flakes in which $LaFeZnO_3$ is surrounded with stacked and scattered particles between the lamellae after doping Cu (Figure 3(d)), Al (Figure 3(e)), and Zn (Figure 3(g)). Exsolved nanoparticles are evenly dispersed on the surface, which are formed from the perovskite lattice structure. For Zn doped materials, the surface active sites of $LaFeO_3$ are rougher with bubble pores, which is conducive to the adsorption of gas to a certain extent. It is expected to show higher catalytic hydrogenation activity[19,20]. The spherical particles became smaller after Ni doping with particle sizes of 20–30 nm (Figure 3(h)).

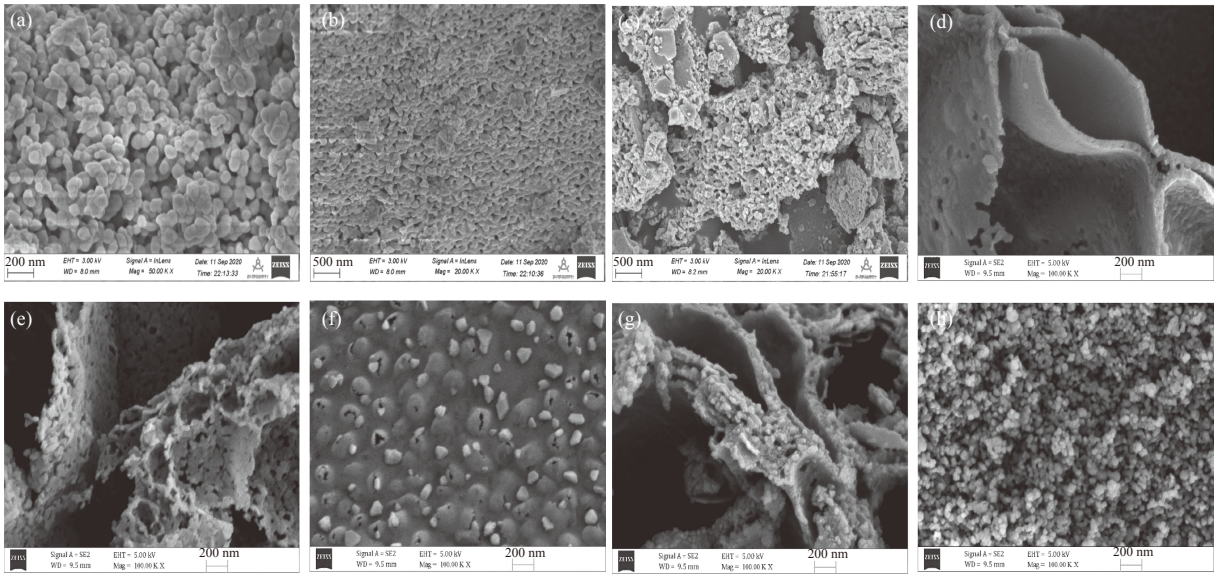

Figure 3 SEM images of $LaFeO_3$ ((a), (b)), $LaFeMnO_3$ (c), $LaFeCuO_3$ (d), $LaFeAlO_3$ (e), $LaFeZrO_3$ (f), $LaFeZnO_3$ (g) and $LaFeNiO_3$ (h)

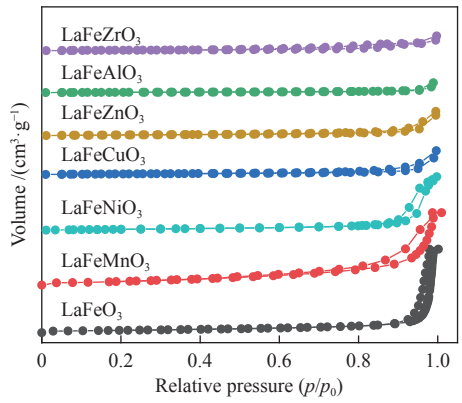

Figure 4 N_2 adsorption-desorption isotherms of various samples

The $LaFeBO_3$ (B =Cu, Zr, Al, Ni, and Zn) catalysts exhibit low BET specific surface areas, as seen in Table 2. Metal doping promotes the formation of small grain size and small specific surface area except for $LaFeMnO_3$ sample, which is related to the weak crystallinity combined with XRD data. The samples with the addition of Zr or Zn have average pore diameters of about 10 nm, which is about a quarter of that of $LaFeO_3$. The type II isotherm with H3 type hysteresis loop indicates the mesoporous structure (Figure 4) suggests the existence of mesoporous structure in perovskite. However, the hysteresis loop of the isotherm is small and the mesoporous structure is limited.

Table 2　Texture properties of $LaFeBO_3$ catalyst samples

Catalyst[a]	BET/ ($m^2 \cdot g^{-1}$)[b]	V_{total}/ ($cm^3 \cdot g^{-1}$)	Average pore diameter[c]/nm
$LaFeO_3$	11.5	0.118	40.96
$LaFeMnO_3$	27.5	0.108	15.68
$LaFeCuO_3$	3.8	0.023	24.83
$LaFeAlO_{3-}$	2.1	0.014	26.74
$LaFeZrO_3$	3.4	0.011	12.55
$LaFeZnO_3$	4.2	0.010	9.58
$LaFeNiO_3$	9.5	0.071	29.80

a: Fresh samples, b: BET desorption cumulative volume,
c: BET desorption average pore diameter

2.3　H_2-TPR experiments

H_2-TPR was employed to investigate the reducibility behavior of various perovskites. There are three peaks for the undoped $LaFeO_3$ at 388, 480, and 620 °C, which could be attributed to the reduction of Fe^{3+} to Fe^{2+} and then the reduction of Fe^{2+} to Fe^0, respectively (see Eq. (3))[21,22], indicating the first transformation of Fe_2O_3 to Fe_3O_4 and further reduction of FeO to Fe. In the case of metal iron-doped $LaFeO_3$, the number of peaks was reduced (Figure 5). When Cu, Zr, Al, Mn, Ni, and Zn are added to the B-site of Fe-based perovskites, low valence Fe ions are formed (see Eq. (4)), which promotes the creation of oxygen vacancies. The impact will be similar if Fe^{3+} is replaced with other metal ions.

$$La^{3+}Fe^{3+}O_3^{2-} \rightarrow La^{3+}_{1-x}Ba^{2+}_xFe^{3+}_{1-x}Fe^{4+}_xO_3^{2-} \quad (3)$$

$$La^{3+}_{1-x}B^{2+}_xFe^{3+}_{1-x}Fe^{4+}_xO_3^{2-} \rightarrow La^{3+}_{1-x}B^{2+}_xFe^{3+}_{1-x+2\delta}Fe^{4+}_{x-2\delta}O^{2-}_{3-\delta}+\delta/2O_2 \quad (4)$$

By replacing the lower valence B^{2+} for Fe^{3+}, the fraction of oxygen vacancy defects and the active oxygen quantity can be changed. By replacing B^{3+} for Fe^{3+}, the properties of transition metal cations and oxygen mobility can be significantly altered. When Ni^{2+} and Cu^{2+} were replaced for Fe^{3+}, increased hydrogen consumption was observed. The materials provide more active oxygen at low temperatures due to the relatively simple redox reaction, which may be attributed to a quicker oxygen diffusion rate in the bulk with increased Fe substitution[23]. Fe is rather easy to be reduced after Cu doping, indicating that the $LaFeCuO_3$ catalyst contains more active oxygen at lower temperature. The $LaFeCuO_3$ catalyst has a quicker oxygen diffusion rate and effectively increases the desolvation of active metals, enhancing the catalytic activity of perovskites. Although the inclusion of Ni also enhances oxygen mobility compared with undoped $LaFeO_3$, the H_2 consumption of Ni varies from Cu, which can be interpreted by different metal reduction ability under H_2 atmosphere. The maximum temperature of Al and Zr doped $LaFeO_3$ increased in the H_2-TPR experiment (Figure 5). The presence of Fe and Zr/Al in the B-site of perovskite structure increases the amount of Fe ions while decreasing the number of oxygen vacancies, which is more likely to stabilize a high oxidation state[10,24].

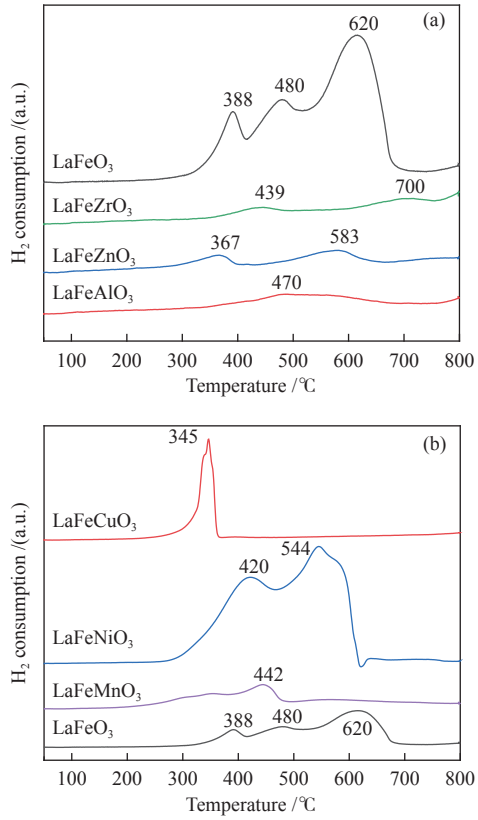

Figure 5　H_2-TPR profiles of the $LaFeBO_3$ samples

The peak region of the H_2-TPR spectra is used to study the reduction behavior for each catalyst. The sequence of initial reduction temperature is $LaFeCuO_3$<$LaFeZnO_3$<$LaFeO_3$<$LaFeMnO_3$<$LaFeNiO_3$<$LaFeZrO_3$<$LaFeAlO_3$. Ni doped perovskite oxide has the biggest peak area, indicating that $LaFeNiO_3$ consumes large amount of hydrogen. At lower temperatures, the addition of Cu or Zn dopant caused the reduction of iron easier than the sole $LaFeO_3$. Metal nanoparticles with a uniform distribution are produced and fixed on the surface of the perovskite matrix after a high-temperature reduction procedure that does not damage the crystal structure. A dopant with catalytic activity and fast reduction is preferred for the process. A heterogeneous structure is formed to produce with a unique synergistic effect to improve the catalytic performance.

2.4 CO_2-TPD measurement

The CO_2-TPD method was used to investigate the change in surface basicity of metal doped Fe based perovskite (Figure 6). Results revealed that doping Al, Mn and other elements at the B position showed a significant effect on the CO_2 desorption of perovskite. The CO_2 desorption curves can be divided into three stages. Weak CO_2 adsorption on the surface of perovskite samples was observed at low temperatures (50 –150 °C). The second range is at 150 –450 °C, indicating that CO_2 adsorption occurred at moderate basic sites. The third range is at about 450 –750 °C, indicating that CO_2 was adsorbed on strong basic site of perovskite. When the B-site was doped with Zn, Zr, and Cu, the content of basic sites on the surface of the corresponding perovskite decreased slightly. Over $LaFeNiO_3$, the amount of CO_2 adsorbed at weakly basic sites was almost disappeared. When Al and Mn were doped at the B site, the amount of adsorbed CO_2 was increased. Therefore, doping Al and Mn could enhance the surface basicity of perovskite[25], while doping Zn, Zr, Cu, and Ni will weaken the surface basicity[26].

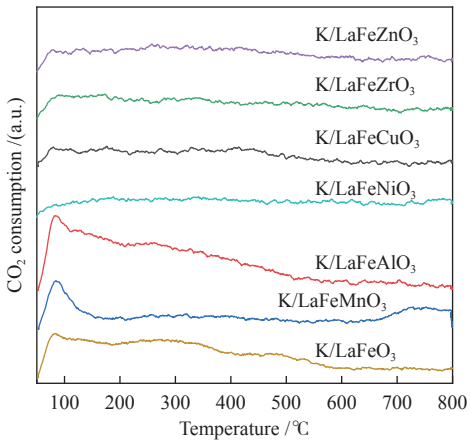

Figure 6 CO_2-TPD profiles of the catalyst samples

2.5 TG experiments

The oxygen migration ability of doped metal perovskite was studied by characterizing the oxygen loss of the catalyst in CO atmosphere (see Figure 7). Except Mn doped $LaFeO_3$, all other samples showed certain oxygen loss, especially for the Zn, Al and Cu doped samples. The properties of Zr doped and undoped samples are basically the same. The weight loss curve of Cu doped catalyst decreased slowly. By simulating the transformation of doped perovskite in reducing atmosphere, it can be judged from the slope in Figure 8 that their oxygen migration rate is greatly affected. When the active particles are exposed to the reducing gas, the active oxygen easily reacts with the reactants, and due to the chemical potential gradient, the oxygen anion penetrates from the bulk to the surface to improve the catalytic efficiency[22,27]. Combined with the catalytic performance, it was found that the oxygen mobility or the generation ability of oxygen vacancy in perovskite had a significant effect on the catalytic activity and product selectivity.

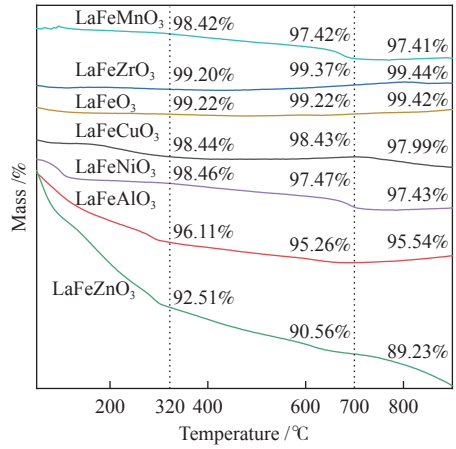

Figure 7 TG analysis of the catalyst samples

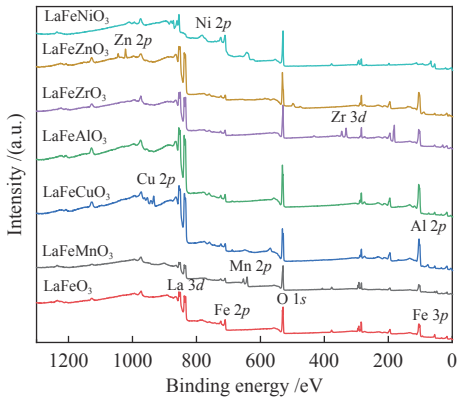

Figure 8 Survey XPS profiles of $LaFeBO_3$ samples

2.6 XPS measurement

The core levels of La 3*d*, Fe 2*p*, Ni 2*p*, Zn 2*p*, Zr 3*d*, Al 2*p*, Cu 2*p*, and Mn 2*p* were investigated and the corresponding spectra are given in Figure 8. La^{3+} inside the perovskite structure has a binding energy (BE) of about 834 eV assigned to La 3*d*[28]. Fe^{3+} cations have a BE of about 710.2 eV, which is followed by a prominent satellite peak in the range 718 –719 eV[29]. Previous research on Fe-based perovskites has revealed that the B-site dopant can change the binding energy of O 1*s*, affecting the olefins selectivity during CO_2 hydrogenation significantly[30]. The creation of oxygen vacancies on the catalyst surface is revealed to be the primary determinant of catalytic activity and product selectivity[31]. The lattice oxygen diffusion maintains the

oxygen vacancy concentration in the catalytic reaction process, and the relative rate of lattice diffusion and surface reaction regulates the product selectivity during the entire reaction process.

The XPS spectra of O 1*s* were shown in Figure 9. The surface oxygen species of the $LaFeBO_3$ perovskite catalysts consist of three over lapping peaks from two chemisorbed surface oxygen species (O^{2-}, O_2^{2-}) and lattice O_2 species (O^{2-})[32]. The O 1*s* spectrum is commonly divided into three components: lattice oxygen species at 529 eV ($O_{lattice}$), surface O-containing species at 531 eV (O_{ads}) as well as 533 eV(O_{-OH}).

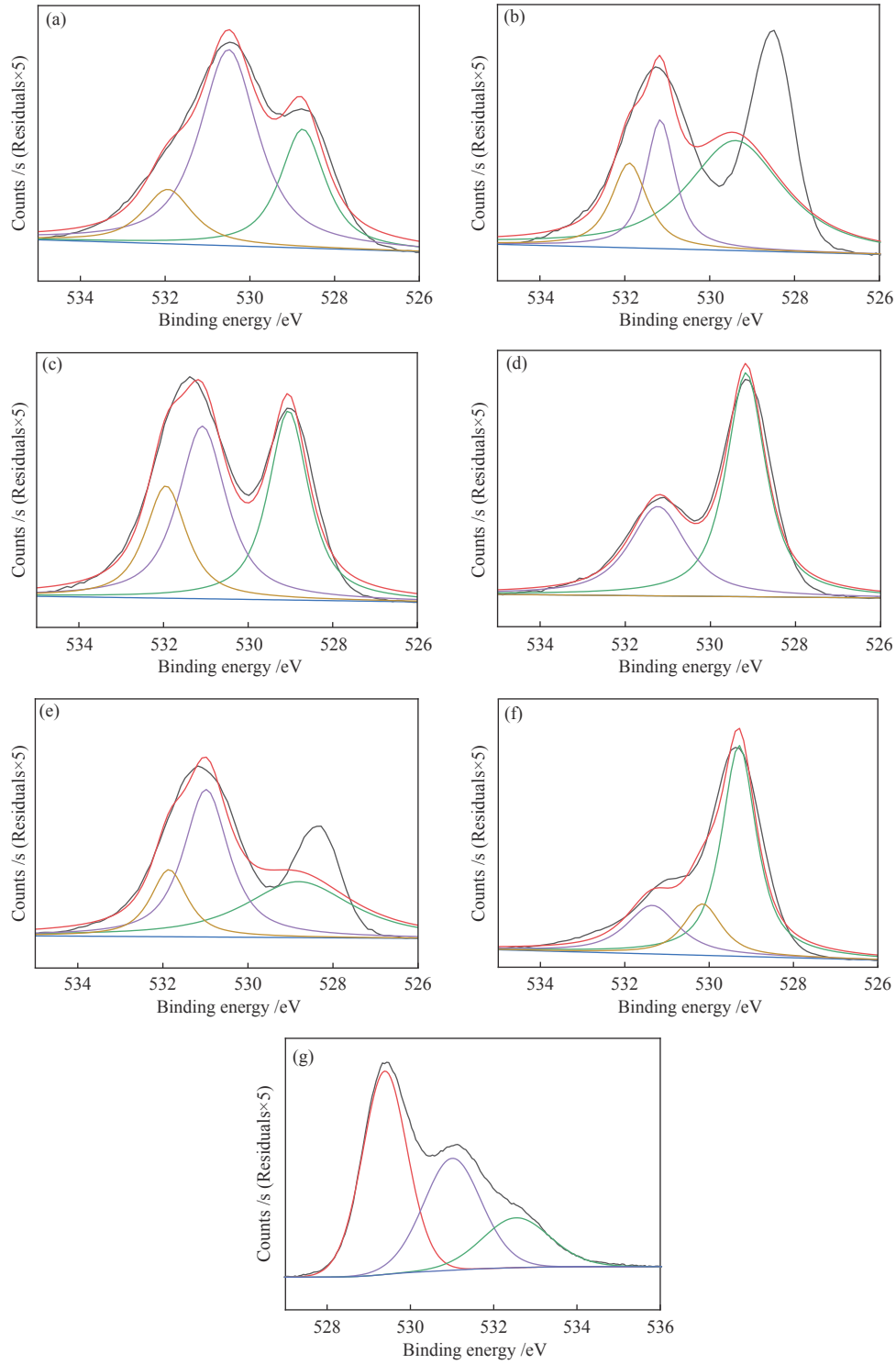

Figure 9　XPS spectra of O 1*s* for different samples
$LaFeO_3$ (a), $LaFeCuO_3$ (b), $LaFeAlO_3$ (c), $LaFeZrO_3$ (d), $LaFeZnO_3$ (e), $LaFeNiO_3$ (f), and $LaFeMnO_3$ (g)

It can be seen that the binding energy of O 1*s* in Fe based perovskite largely depends on the type of B-doped metals, which has a great effect on CO_2 hydrogenation. The difference in the binding energy of O^{2-} is due to the electronegativity difference of metal cations interacting with O anions. $LaFeBO_3$ perovskite catalysts contained lattice oxygen species with varying O 1*s* BEs and demonstrated a remarkably different selectivity of olefins in CO_2 hydrogenation, depending on the B site components[19]. In Figure 10, the Fe 2*p* peaks in the perovskite are concentrated at 709−711 eV and 722−724 eV, which is attributed to Fe^{3+} characteristic peak. Peak located at (717±0.4) eV belongs to the α-Fe_2O_3 satellite peak. Affected by metal doping, the α-Fe_2O_3 satellite peak disappears, thus the chemical environment around Fe changes greatly, which in turn affects the hydrogenation reaction behavior.

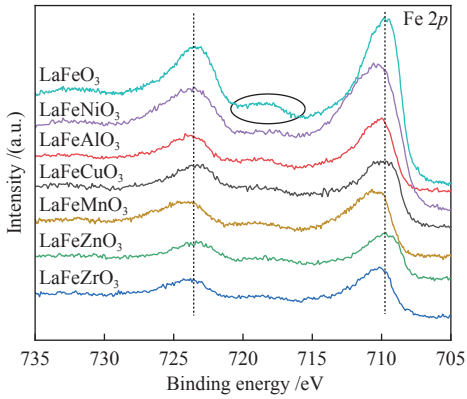

Figure 10 XPS spectra of Fe *2p* for different samples

In conclusion, surface oxygen vacancies generated by the interaction of lattice oxygen with CO_2 were filled with adsorbed surface oxygen and bulk lattice oxygen species. As a result, oxygen mobility in perovskites has a considerable impact on the catalytic activity and product selectivity. The surface oxygen concentration or oxygen vacancy concentration, which is determined by the bulk oxygen concentration and the relative rate of lattice oxygen transport compared to the surface reaction, is a major determinant of the catalytic performance of perovskites in CO_2 hydrogenation[33]. Besides, the chemical compositions and states of catalysts have been investigated in this study. These values were investigated and calculated from ICP and XPS spectra, as shown in Table 3. The bulk compositions of Fe and B species for $LaFeBO_3$ showed slightly lower surface concentrations of Fe and B species. The internal element content shows divergence from surface, which correlates the difference of Cu and Ni reduction ability in previous H_2-TPR experiment explicitly.

Table 3 Surface composition of the catalysts determined by XPS

Sample	Surface element content w_{mol}/%			Fe/B	Fe/B*
	Fe	O	B		
$LaFeMnO_3$	3.81	59.01	4.09	0.93	0.69
$LaFeCuO_3$	5.87	59.29	6.09	0.96	0.98
$LaFeAlO_3$	4.15	60.1	6.03	0.69	0.59
$LaFeZrO_3$	4.77	54.95	8.02	0.59	0.53
$LaFeZnO_3$	3.8	57.41	4.67	0.81	0.87
$LaFeNiO_3$	7.48	59.74	8.05	0.93	0.89

* Determined by ICP

2.7 Catalytic performance

The catalytic performance for CO_2 hydrogenation is shown in Table 4. $K/LaFeO_3$ has the lowest activity with methane as the main product. However, with the addition of metal dopants, the catalytic activity increased. Metal doping is beneficial to expose more active sites and promote the CO_2 hydrogenation over $LaFeBO_3$ catalysts. Cu and Zn modified perovskite exhibit higher activity with 27%–41% of C_2–C_4 olefins in total hydrocarbons.

Table 4 Catalytic activity of different catalysts

Catalyst sample	CO_2 conv. /%	CO sel. /%	Hydrocarbon distribution C/%				O/P
			CH_4	$C_2^= - C_4^=$	$C_2^0 - C_4^0$	C_{5+}	
$K/LaFeO_3$	5.6	24.2	90.4	0	9.6	0	0
$K/LaFeMnO_3$	25.3	85.0	51.6	19.3	15.1	14.1	1.3
$K/LaFeCuO_3$	35.6	62.3	41.3	27.2	22.7	8.8	1.2
$K/LaFeZrO_3$	7.4	81.5	77.8	14.1	8.1	0	1.5
$K/LaFeAlO_3$	8.2	87.6	78.9	10.0	11.1	0	0.9
$K/LaFeNiO_3$	30.3	80.3	69.9	10.9	9.3	10	1.2
$K/LaFeZnO_3$	48.5	25.7	15.62	41.0	16.9	26.5	2.4

Reaction conditions: H_2/CO_2 = 3, 320 °C, 2.0 MPa, 1000 h^{-1} and TOS=24 h

The $LaFeBO_3$ catalysts have a strong RWGS activity aside from Zn doping. CO selectivity reach as high as 80%−92%. The varied activities of $LaFeBO_3$ catalysts are most likely caused by the distinct characteristics of the lattice oxygen species, which are governed by the metal elements in the B sites. Nanoparticles and sintering are inhibited by the "anchoring" of the reducible lattice cations, which migrate and penetrate to form nanoparticles and diffuse on the surface of the materials[18,25]. The doped Zn and Cu boost the activation of oxygen anion in reducing gas and increase the number of exposed particles. Due to the presence of a chemical potential gradient, the active oxygen rapidly combines with it and permeates from the bulk phase to the surface, boosting catalytic activity and facilitating in the production of olefins.

3 Conclusions

Sol-gel method was utilized to successfully prepare Cu, Zr, Al, Mn, Ni, and Zn-doped $LaFeO_3$ perovskites, and the potential of $LaFeBO_3$ perovskites as oxygen carriers for CO_2 hydrogenation was investigated. Increased catalytic activity are expected for $LaFeBO_3$ perovskites. Doping the catalyst with a second metal/metal oxide improved olefin selectivity by producing a highly active surface. The perovskites feature a tunable host lattice that allows for effective CO_2 adsorption, activation, and lattice oxygen migration, as well as the ability to improve catalytic activity. CO_2 conversion was facilitated by oxygen species in the surface lattice. Substituting Cu and Zn for Fe at the B site, in particular, considerably enhanced oxygen mobility and displayed high activity in CO_2 hydrogenation. In addition, Zn doped perovskite showed high selectivity to light olefins for CO_2 hydrogenation.

References

[1] DO T N, KIM J. Green C_2-C_4 hydrocarbon production through direct CO_2 hydrogenation with renewable hydrogen: Process development and techno-economic analysis[J]. Energy Convers Manage, 2020, **214**: 112866.

[2] GAO P, DANG S S, LI S G, BU X N, LIU Z Y, QIU M H, YANG C G, WANG H, ZHONG L S, HAN Y, LIU Q, WEI W, SUN Y H. Direct production of lower olefins from CO_2 conversion via bifunctional catalysis[J]. ACS Catal, 2018, **8**(1): 571−578.

[3] WANG D, XIE Z H, POROSOFF M D, CHEN J G. Recent advances in carbon dioxide hydrogenation to produce olefins and aromatics[J]. Chem, 2021, **7**(9): 2277−2311.

[4] ZHU H Y, ZHANG P F, DAI S. Recent advances of lanthanum-based perovskite oxides for catalysis[J]. ACS Catal, 2015, **5**(11): 6370−6385.

[5] LI D Y, XU R D, LI X Y, LI Z Q, ZHU X, LI K Z. Chemical looping conversion of gaseous and liquid fuels for chemical production: A review[J]. Energy Fuels, 2020, **34**(5): 5381−5413.

[6] QIU Y, MA L, ZENG D W, LI M, CUI D X, LV Y L, ZHANG S, XIAO R. Efficient CO_2 to CO conversion at moderate temperatures enabled by the cobalt and copper co-doped ferrite oxygen carrier[J]. J Energy Chem, 2020, **46**: 123−132.

[7] SHARMA P, ELDER T, GROOM L H, SPIVEY J J. Effect of structural promoters on Fe-Based Fischer-Tropsch synthesis of biomass derived syngas[J]. Top Catal, 2013, **57**(6/9): 526−537.

[8] TIEN THAO N, SON L T. Production of cobalt-copper from partial reduction of La(Co, Cu)O_3 perovskites for CO hydrogenation[J]. J Sci-Adv Mater and Dev, 2016, **1**(3): 337−342.

[9] LIU Y, CHEN J F, BAO J, ZHANG Y. Manganese-modified Fe_3O_4microsphere catalyst with effective active phase of forming light olefins from syngas[J]. ACS Catal, 2015, **5**(6): 3905−3909.

[10] ZHAN H J, LI F, GAO P, ZHAO N, XIAO F K, WEI W, ZHONG L S, SUN Y. Methanol synthesis from CO_2 hydrogenation over La-M-Cu-Zn-O (M=Y, Ce, Mg, Zr) catalysts derived from perovskite-type precursors[J]. J Power Sources, 2014, **251**: 113−121.

[11] DING J, ZHAO W X, ZI L T, XU X, LIU Q, ZHONG Q, XU Y. Promotional effect of ZrO_2 on supported FeCoK catalysts for ethylene synthesis from catalytic CO_2 hydrogenation[J]. Int J Hydrogen Energy, 2020, **45**(30): 15254−15262.

[12] ELISHAV O, SHENER Y, BEILIN V, LANDAU M V, HERSKOWITZ M, SHTER G E, GRADER G S. Electrospun Fe-Al-O nanobelts for selective CO_2 hydrogenation to light olefins[J]. ACS Appl Mater Inter, 2020, **12**(22): 24855−24867.

[13] GAO Q, MENG J, YANG Y, LIN Q Y, LU Y F, WEI X, LI J X, HAN G R, ZHANG Z. Zirconium doping in calcium titanate perovskite oxides with surface nanostep structure for promoting photocatalytic hydrogen evolution[J]. Appl Surf Sci, 2021, **542**: 148544.

[14] WEI C Y, TU W F, JIA L Y, LIU Y Y, LIAN H L, WANG P, ZHANG Z Z. The evolutions of carbon and iron species modified by Na and their tuning effect on the hydrogenation of CO_2 to olefins[J]. Appl Surf Sci, 2020, **525**: 146622.

[15] HARE B J, MAITI D, RAMANI S, RAMOS A E, BHETHANABOTLA V R, KUHN J N. Thermochemical conversion of carbon dioxide by reverse water-gas shift chemical looping using supported perovskite oxides[J]. Catal Today, 2019, **323**: 225−232.

[16] LINDENTHAL L, POPOVIC J, RAMESHAN R, HUBER J, SCHRENK F, RUH T, NENNING A, LÖFFLER S, OPITZ A K, RAMESHAN C. Novel perovskite catalysts for CO_2 utilization-exsolution enhanced reverse water-gas shift activity[J]. Appl Catal B: Environ, 2021, **292**: 120183.

[17] LINDENTHAL L, RAMESHAN R, SUMMERER H, RUH T, POPOVIC J, NENNING A, LÖFFLER S, OPITZ A K, BLAHA P, RAMESHAN C. Modifying the surface structure of perovskite-based catalysts by nanoparticle exsolution[J]. Catalysts, 2020, **10**(3): 268−282.

[18] CHANG H, BJØRGUM E, MIHAL O, YANG J, LEIN H L, GRANDE T, RAAEN S, ZHU Y A, HOLMEN A, CHEN D. Effects of oxygen

mobility in La-Fe-based perovskites on the catalytic activity and selectivity of methane oxidation[J]. ACS Catal, 2020, **10**(6): 3707−3719.

[19] WU J X, ZHENG Y S, DACQUIN J P, DJELAL N, CORDIER C, DUJARDIN C, GRANGER P. Impact of dual calcium and manganese substitution of La-deficient perovskites on structural and related catalytic properties: Future opportunities in next three-way-catalyst generation[J]. Appl Catal A: Gen, 2021, **619**: 118137.

[20] ABBAS M, ZHANG J, MANSOUR T S, CHEN J G. Hierarchical porous spinel MFe_2O_4 (M=Fe, Zn, Ni and Co) nanoparticles: Facile synthesis approach and their superb stability and catalytic performance in Fischer-Tropsch synthesis[J]. Int J Hydrogen Energy, 2020, **45**(18): 10754−10763.

[21] YANG Q L, LIU G L, LIU Y. Perovskite-type oxides as the catalyst precursors for preparing supported metallic nanocatalysts: A review[J]. Ind Eng Chem Res, 2018, **57**(1): 1−17.

[22] WU M D, CHEN S Y, XIANG W G. Oxygen vacancy induced performance enhancement of toluene catalytic oxidation using $LaFeO_3$ perovskite oxides[J]. Chem Eng J, 2020, **387**: 124101.

[23] FANG Y Z, LIU Y, ZHANG L H. $LaFeO_3$-supported nano Co-Cu catalysts for higher alcohol synthesis from syngas[J]. Appl Catal A: Gen, 2011, **397**(1/2): 183−191.

[24] YIN K J, SHEN Y L. Theoretical insights into CO_2 hydrogenation to HCOOH over $Fe_xZr_{1-x}O_2$ solid solution catalyst[J]. Appl Surf Sci, 2020, **528**: 146926.

[25] SIM Y, KWON D, ANA S, HAB J M, OHC T S, JUNG J H. Catalytic behavior of ABO_3 perovskites in the oxidative coupling of methane[J]. Mol Catal, 2020, **489**: 110925.

[26] SHESHKO T F, MARKOVA E B, SHARAEVA A A, KRYUCHKOVA T A, ZVEREVA I A, CHISLOVA I V, YAFAROVA L V. Carbon monoxide hydrogenation over Gd (Fe/Mn) O_3 perovskite-type catalysts[J]. Petrol Chem, 2019, **59**(12): 1307−1313.

[27] MATTSSON A, LEJON C, BAKARDJIEVA S, ŠTENGL V, ÖSTERLUND L. Characterisation, phase stability and surface chemical properties of photocatalytic active Zr and Y co-doped anatase TiO_2 nanoparticles[J]. J Solid State Chem, 2013, **199**: 212−223.

[28] EZBIRI M, BECATTINI V, HOES M, MICHALSKY R, STEINFELD A. High redox capacity of Al-Doped $La_{1-x}Sr_xMnO_{3-\delta}$ perovskites for splitting CO_2 and H_2O at Mn-enriched surfaces[J]. ChemSusChem, 2017, **10**(7): 1517−1525.

[29] GROSVENOR A P, KOBE B A, BIESINGER M C, MCINTYRE N S. Investigation of multiplet splitting of Fe 2*p* XPS spectra and bonding in iron compounds[J]. Surf Interface Anal, 2004, **36**(12): 1564−1574.

[30] WU J X, ZHENG Y S, DACQUIN J P, DJELAL N, CORDIER C, DUJARDIN C, GRANGER P. Impact of dual calcium and manganese substitution of La-deficient perovskites on structural and related catalytic properties: Future opportunities in next three-way-catalyst generation[J]. Appl Catal A: Gen, 2021, **619**(11): 118−137.

[31] XI X Y, ZENG F, ZHANG H, WU X F, REN J, BISSWANGER T, STAMPFER C, HOFMANN J P, PALKOVITS R, HEERES H J. CO_2 hydrogenation to higher alcohols over K-promoted bimetallic Fe–In catalysts on a Ce-ZrO_2 support[J]. ACS Sustainable Chem Eng, 2021, **9**(18): 6235−6249.

[32] SHI J M, CHANG Y, TANG Y S, WANG X B, WANG X F, ZHANG X C, CAO J L. Hydrogenated $LaFeO_3$ with oxygen vacancies for enhanced visible light photocatalytic performance[J]. Ceram Inter, 2020, **46**(4): 5315−5322.

[33] ZHANG X H, PEI C L, CHANG X, CHEN S, LIU R, ZHAO Z J, MU R T, GONG J L. FeO_6 octahedral distortion activates lattice oxygen in perovskite ferrite for methane partial oxidation coupled with CO_2 splitting[J]. J Am Chem Soc, 2020, **142**(26): 11540−11549.

金属掺杂对 LaFe 基钙钛矿催化 CO_2 加氢制低碳烯烃性能影响

马利海, 高新华, 张建利*, 马晶晶, 胡修德, 郭庆杰*

(宁夏大学 省部共建煤炭高效利用与绿色化工国家重点实验室 化学化工学院, 宁夏 银川 750021)

摘 要: 通过溶胶-凝胶法和浸渍法制备 K/$LaFeBO_3$ (B =Cu、Zr、Al、Mn、Ni、Zn) 钙钛矿催化剂, 结合 SEM、XRD、BET、H_2-TPR、CO_2-TPD、TG、XPS 等表征, 探究了金属掺杂对 LaFe 基钙钛矿催化 CO_2 加氢制备低碳烯烃性能的影响。结果表明, Cu 和 Zn 的加入有利于提高 Fe 分散度并降低还原温度, 同时低温下氢的脱附增加且碱性位增多。氧空位迁移变化对催化活性和烯烃选择性有重要影响, 当 Cu 和 Zn 在 B 位取代 Fe 时, 氧迁移率增加明显, 具有较低结合能的表面晶格氧富集, 显著提高了催化活性, 促进了低碳烯烃生成。

关键词: 二氧化碳加氢; 钙钛矿; $LaFeBO_3$ 催化剂; 氧迁移

中图分类号: TQ546 **文献标识码:** A